MIMO channel measurements for personal area networks

Johansson, Anders J; Kåredal, Johan; Tufvesson, Fredrik; Molisch, Andreas

Published in:
[Host publication title missing]

DOI:
10.1109/VETECS.2005.1543272

2005

MIMO Channel Measurements for Personal Area Networks

Anders J Johansson[1], Johan Karedal[1], Fredrik Tufvesson[1], and Andreas F. Molisch[1,2]

[1] Department of Electroscience, Lund University, Box 118, SE-221 00 Lund, Sweden,

[2] Mitsubishi Electric Research Labs, 201 Broadway, Cambridge, MA 02139, USA.

Email: {Anders.J.Johansson, Johan.Karedal, Fredrik.Tufvesson, Andreas.Molisch}@es.lth.se

***Abstract*— This paper analyzes MIMO propagation channels for personal area networks. Such channels show important differences to propagation channels in wide-area networks, due to the different environments in which the systems are operated, as well as due to different mobility models, ranges, and presence of humans in the environment, and the impact of the antenna arrangement. We present results from a recent measurement campaign for this type of channel. We first analyze the requirements for measurement setups, especially in terms of different positions and orientations of the antenna arrays, to obtain meaningful results. We then analyze the measured data and present results for path loss, power delay profiles, spatial correlation and temporal correlation.**

I. Introduction

In recent years there has been an increase of interest in wireless systems with high data rates but small coverage area. Such systems, commonly known as "personal area networks" (PANs), are often defined as a network where transmitter and receiver are separated no more than 10 m, and are usually within the same room. Due to the high required data rates, innovative transmission schemes have been proposed: both ultrawideband techniques [1], [2] and MIMO (multiple-input−multiple-output) systems seem suitable. Among other investigations, the European Union has commissioned the MAGNET project that investigates different approaches to realizing PANs.

MIMO systems, i.e., systems with multiple antenna elements at both link ends, promise high spectral efficiency and thus high data rates by allowing the transmission of multiple data streams without additional spectral resources [3], [4], [5]. For this reason, many theoretical as well as experimental investigations have been performed on different aspects of MIMO in the last 10 years [6]. It has been shown repeatedly that the wireless propagation channel has a key impact on both the information-theoretical limits and the performance of practical MIMO systems [7].

Past measurements and modeling of MIMO propagation channels concentrated mostly on scenarios that correspond to wide-area (cellular) networks [8] and wireless local area networks [9]. Those measurements have found it useful to separate the impact of the antennas from the channel, and describe the channel by its double-directional impulse response [10], or the transfer function matrix in the absence of human beings close to the "mobile station".[1] However, this approach is impractical in PANs, especially for hand-held and body-worn devices. A double-directional channel characterization is based on extracting the parameters (delay, angle-of-arrival, angle-of-departure) of the multipath components (MPCs) and requires the use of large antenna arrays. Only those guarantee a sufficient number of spatial samples, which are a prerequisite for the high-resolution algorithms that extract the MPC parameters [12], [13]. At 2.6 GHz, an 8-element uniform linear array is about 0.5 m long. It is obviously impossible to mount such an array on a person to achieve a "body-worn device", including the effect of the human. It is thus preferable to analyze the combined effect of channel, antennas, and human operators of the mobile station, using the same antenna configurations for the measurements that would also be used for the actual operation.

In the current paper, we present the results of a recent measurement campaign that deals specifically with MIMO for PANs, and has the following characteristics:

- Measurements are done in a modern office building at a carrier frequency of 2.6 GHz for dual-polarized arrays.
- Both nomadic mobility (Tx and Rx stationary) with stationary surroundings, nomadic mobility with temporally varying surroundings (moving people), and movement of the devices, are taken into account.
- The impact of typical antenna arrangements (antennas on the back of a laptop and antennas in a Personal Digital Assistant, PDA) is taken into account.
- A generic channel model that is especially suited for the considered scenarios, is developed and parameterized.

II. Measurement Setup

A. Antenna Arrays

Measurements were done with the RUSK LUND channel sounder that performs MIMO measurements based on the "switched array" principle [14]. The measurements were performed at a center frequency of 2.6 GHz and using a test signal with a bandwidth of 200 MHz. The RUSK sounder allows to adjust the length of the test signal, and for these measurements a value of 1.6 μs was used, corresponding to a resolvable "excess runlength" of multipath components of 480 m, which was more than enough to avoid overlap of consecutive impulse responses. Both the receiver and the transmitter port were connected to a multiplexer (MUX), which switched the signal to one of 32 possible connectors.

Three different antennas (arrays) were used; a fixed device (FD), such as an indoor base station, a portable computer (PC)

[1] An exception is, e.g., the recent paper [11] that analyzes the impact of humans on the transfer function in wireless LANs.

0-7803-8887-9/05/$20.00 (c)2005 IEEE

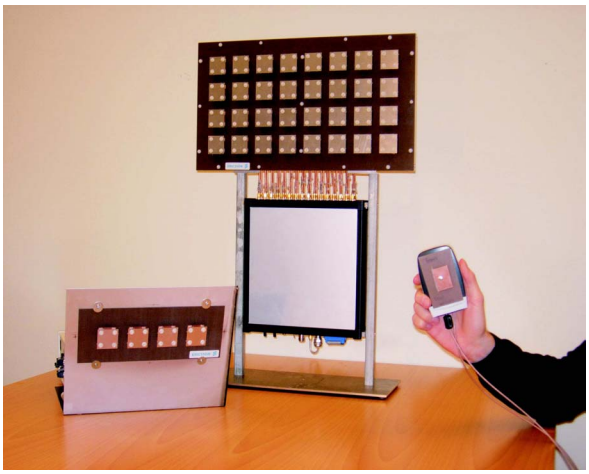

Fig. 1. The antennas used in the measurements. The PC on the left, the fixed device (FD, with multiplexer) in the middle and the handheld (HH) device on the right.

and a hand-held device (HH). Photographs of the antennas can be seen in Fig. 1. As a fixed device, we used a flat-panel patch array, consisting of 8 by 4 dual-polarized antenna elements. Out of those 64 available antenna ports, only the 32 ports corresponding to the middle two rows of the array were sampled. The top and bottom rows ports were all terminated with 50 Ω. The PC antenna array consisted of one row of 4 similar dual-polarized patch antennas; identical to those used on the fixed device. The array was mounted on a chassis simulating a placement on the backside of the screen of a laptop computer. During the measurements, the screen was tilted at 105 degrees, corresponding to a "normal usage" scenario. The receiver MUX was placed at the position of the keyboard. Furthermore we used a handheld device with two patch antennas, one on the front and one on the back. These antennas were single polarized: when holding the device upright, the front antenna was horizontally polarized, and the back antenna was vertically polarized. These polarizations became slanted in the "in-use" position utilized in the measurements.

B. Measurement Locations

The measurements were performed in the E-building of LTH, Lund University. It is a modern office building made of reinforced concrete, with gypsum wallboards separating the different offices. Three different scenarios were measured; from FD to PC, from FD to HH and from PC to HH. For each scenario a number of antenna positions were selected in order to achieve LOS as well as NLOS measurements. Fig. 2 shows the positions for the FD to PC/HH scenario. During the measurements, all office doors were open and there were basically no movements in the corridor. The PC was placed at typical working positions at existing desks in different offices. The HH device was held in hand at a typical palm-top operating position in front of the chest. Finally, the FD was placed close to the ceiling.

We analyze both line-of-sight (LOS) and non-LOS (NLOS) scenarios. In the following, we define LOS as were there was a direct optical path between Tx and Rx, i.e., the Rx could be seen from Tx. The directions of the antennas does not affect the LOS definition (i.e., measurements with Rx and Tx in the same office, but facing away from each other, counts as LOS) and neither does the possible obstruction by the person carrying the HH device, since that person is considered a part of the HH antenna. Note also that the height difference between FD and PC/HH should be considered, e.g., when evaluating the results for the smaller distances.

C. The FD-PC and FD-HH Scenario

The FD-PC and FD-HH measurements were done simultaneously, with the PC antenna array located on a desk and the HH being held in one hand by a person sitting in front of the PC. Antenna measurement positions were selected amongst the positions of Fig. 2 to create 65 different measurement positions (i.e., Tx-Rx separations). For each measurement position 8 measurements of the array impulse response were taken in the static measurements. For the FD-PC scenario, each of those 8 measurements was characterized by a translation (by 40 cm) and/or a 180 degree rotation with respect to the reference position. For the HH scenario, each of the 8 measurements was characterized by a translation only. Using the 8 different measurements, as well as the large Tx arrays (remember that the FD has 32 antenna ports) gives a large number of spatial samples that improves the statistical reliability of the measurement results. Note that the rotation of the measurement device leads to a shadowing, which is therefore included in the statistics of the observed signal.

The dynamic measurements in this scenario were performed in a time-varying *channel,* where the transmit and receive antennas were static but a person was walking with a speed of approximately 1.5 m/s, eastward along the corridor in Fig. 2, past the transmitter (only one Tx position was used).

D. The PC-HH Scenario

Both static and dynamic measurements were made for this scenario, in which the PC antenna array was used as transmitter. The static measurements included 5 Tx-positions (Rx positions 4, 9, 10, 19 and 20 in Fig. 2 were also used as Tx positions in this scenario) and an average of 5 Rx-positions per Tx position. These measurements were made for LOS only. As in the FD to PC/HH scenario, 8 consecutive measurements were made for each receiver positions, with small offsets in the position of the HH.

Dynamic measurements were made with the HH as a mobile receive antenna. All 5 (static) Tx positions were used. The HH was held by a person walking along the corridor at a speed of approximately 1.5 m/s and then making a turn into the office containing the transmitter. The walk included approximately 3 seconds of NLOS and 3 seconds of LOS.

E. Data Processing

The RUSK channel sounder measures channel transfer functions; these were converted to impulse responses by means of an inverse Fourier transform using a Hanning window. From the instantaneous power delay profiles (PDPs), i.e., the squared magnitudes of the impulse responses, the average PDP (APDP) was determined as the average of the $N_r \times N_t$ PDPs, where N_r is

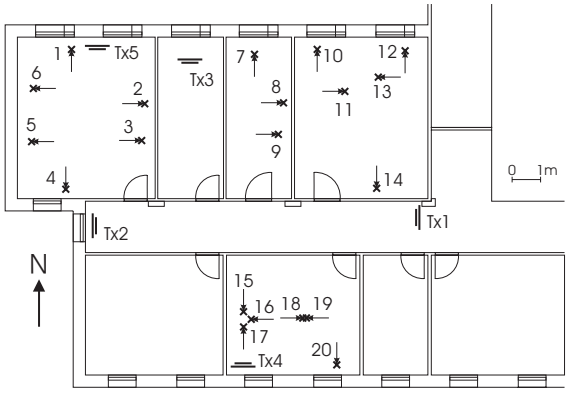

Fig. 2. A site map of the measurement positions for the FD-PC/HH measurements. The Tx positions for the FD-PC/HH measurements are labelled "Tx" whereas the Rx positions (used in all campaigns) are unlabelled. The arrows indicate the direction of each Rx antenna setup.

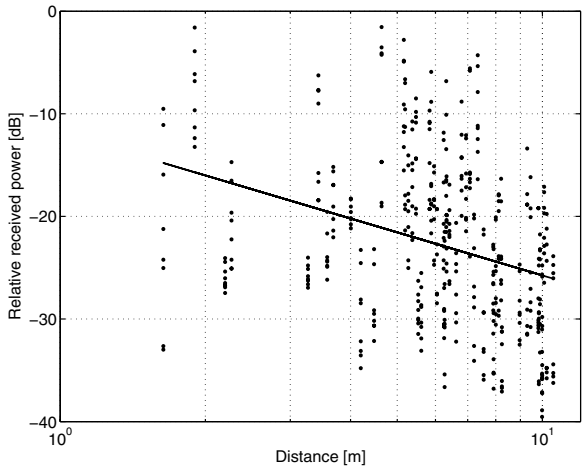

Fig. 3. Scatter plot of the recieved power versus distance for the FD-PC hh NLOS channels.

the number of receive antennas and N_t is the number of transmit antennas, belonging to a certain measurement.

Due to the short distances measured, and the high dynamic range of the measurement equipment, all measurement results showed a very good dynamic range. In the postprocessing, only values of the PDP within 30 dB of the peak value were considered; all other parts were neglected and set to zero.

An important observation of previous measurement campaigns is that the arriving signal can be written as the sum of the contributions from different "clusters" of scatterers [15]. We defined a cluster if it gave rise to a local maximum in the APDP if it had a power of at least 5 dB above the previous local minimum. With this definition, all measurements contained only one cluster. Note that due to the idiosyncrasies of measuring PAN channels, it is not possible to use the angular domain for a more refined identification of clusters.

III. Measurement Results

In this section we present the results from our measurement campaign, and develop a statistical channel model based on those results. Due to space restrictions, we can only show some exemplary plots (for the PC-FD NLOS case), but the parameterization of the channel model that we give (see also the tables below) is based on all the measurement results.[2]

A. Pathloss Modeling

Fig. 3 shows a scatter plot of the received power as function of distance for the co-polarized horizontal to horizontal (hh) PC-FD NLOS scenario. The received power is here normalized by a reference measurement: 0 dB correspond to the power that was received at a distance $d_0 = 2.5$ m in an anechoic chamber.

[2]During the measurement evaluation, it turned out that the multiplexer port used for one of the HH antennas was faulty. For this reason, parameterization is only available for the "hh" and the "vh" polarizations in the PC-HH and FD-HH measurements. However, due to the multitude of antennas at the transmitter as well as the number of different measurements in each "location", conclusions can still be drawn regarding the properties of co-polarized and cross-polarized components.

TABLE I

Estimated pathloss n-exponents for the different scenarios.

		FD-PC	FD-HH	PC-HH
LOS:	hh	0.12	0.28	0.46
	vv	0.00	–	–
	hv	0.41	–	–
	vh	0.63	0.49	0.48
NLOS:	hh	1.40	1.99	–
	vv	1.22	–	–
	hv	1.62	–	–
	vh	1.52	2.04	–

We distinguish between three different loss components for the path loss; the distance dependent path loss, large scale fading due to orientation and large position shifts of the device, and small scale fading to account for small distance variations between the considered antenna elements. It is well established to use a power-law for the distance-dependent pathloss, together with log-normal variations to account for the large-scale fading

$$PL\left(d\right) = \overline{PL}\left(d_0\right) + 10n\log_{10}\left(\frac{d}{d_0}\right) + X_\sigma$$

where $\overline{PL}\left(d_0\right)$ is the pathloss at the reference distance d_0. In Fig. 3 we also provide a linear fit (on a logarithmic scale) obtained from minimum squared error criterion. In this case, a path loss exponent $n = 1.40$ is obtained. Estimated path loss exponents for the different cross- and co-polarized channels are given in Table I. Note that in the FD-PC measurements, the shadowing is created both by rotations and different measurement locations, while for the other two scenarios it is created by different locations only, see Section II-C.

We see that there is a slight difference in the path-loss exponents between the cross- and co-polarized channels. Note however that the distance dependent pathloss in the considered range, $1 - 10$ m, has a minor influence compared to the large scale fading, and due to this effect, the exponent is sensitive to insufficient sample size and other statistical artefacts.

The large scale fading is used to model the influence of the orientation and position of the device. Both these have a major

TABLE II

PARAMETERS FOR THE LARGE SCALE FADING IN dB.

		FD-PC σ_X	FD-HH σ_X	PC-HH σ_X
LOS:	hh	5.24	4.68	3.69
	vv	4.41	–	–
	hv	3.70	–	–
	vh	4.35	3.26	3.76
NLOS:	hh	7.76	5.46	–
	vv	6.77	–	–
	hv	5.84	–	–
	vh	5.70	4.39	–

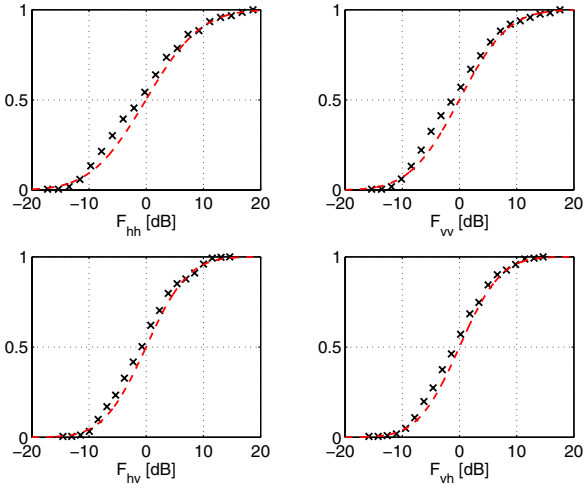

Fig. 4. Cumulative distribution functions of the large scale fading for the FD-PC NLOS measurements for the four different polarizations. The x:es are from the measured data whereas the dashed lines are best-fit Gaussian distributions.

influence on the received power in our measurements, since the typical usage positions of a laptop sometimes implies that the antenna array is close to (and aimed at) a wall. The shadowing can be modeled as log-normally distributed around the distance-dependent pathloss, as demonstrated in Fig. 4, with zero-mean, and a standard deviation σ_X as given by Table II.

B. Power Delay Profiles

As mentioned earlier, all APDPs contain only a single (main) cluster. The cluster shape is best described by a single exponential decay, i.e.,

$$P(\tau) = |\beta|^2 e^{-\tau/\gamma}$$

where γ is the decay time constant, and $|\beta|^2$ the power gain. Fig. 5 shows a typical APDP (solid line) as well as a linear regression line (on a dB scale), corresponding to the one-sided exponential decay. We found that, for our scenarios, the decay time constant γ does not exhibit any deterministic dependence on the distance (note that other measurement campaigns finding such a distance dependence usually analyze larger distances between Tx and Rx and are thus not comparable to our PAN scenarios). On the other hand, we found statistical variations of the decay time constant around its mean. A normal distribution gives the best fit (see Fig. 6); the mean m_γ and standard deviation σ_γ are given in Table III.

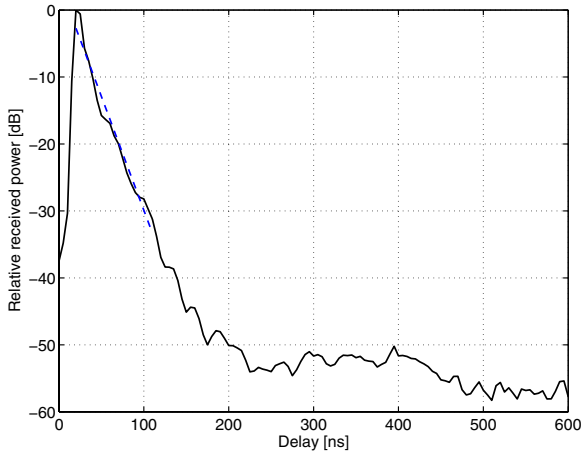

Fig. 5. A typical power delay profile for the NLOS measurement of the FD-PC scenario, hh polarized channels only. The dashed line is a best-fit regression line.

TABLE III

MEAN AND STANDARD DEVIATION IN ns FOR THE GAUSSIAN DISTRIBUTED DECAY TIME CONSTANTS.

		FD-PC		FD-HH		PC-HH	
		m_γ	σ_γ	m_γ	σ_γ	m_γ	σ_γ
LOS:	hh	10.2	1.41	9.61	1.71	10.7	1.53
	vv	10.2	1.35	–	–	–	–
	hv	11.3	1.17	–	–	–	–
	vh	10.9	1.25	10.6	1.18	11.6	1.58
NLOS:	hh	11.6	2.15	11.8	1.85	–	–
	vv	12.1	1.90	–	–	–	–
	hv	13.2	1.72	–	–	–	–
	vh	13.1	1.65	13.0	1.50	–	–

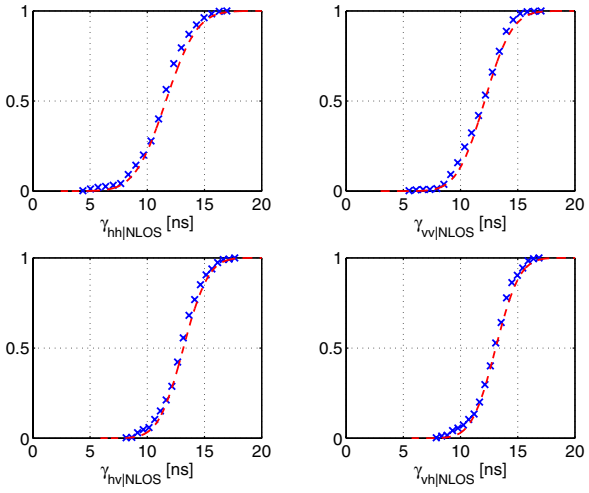

Fig. 6. Cumulative distribution functions of the decay time constants γ for the four different polarizations. The x:es are the measured data, whereas the dashed lines are best-fit Gaussian distributions.

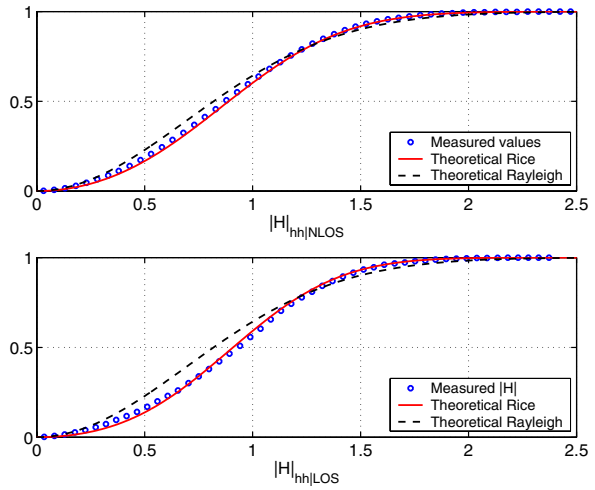

Fig. 7. Cumulative distribution functions of the amplitudes of the hh channels for the FD-PC scenario, NLOS and LOS.

The amplitude gains $|\beta|$ are approximated to have a Rayleigh distribution for NLOS and a Ricean distribution for LOS (see Fig. 7). The best fit is actually to a Ricean distribution in both cases, with estimated Ricean K-factors (using the method by Greenstein *et al*. [16]) in the range of $1.02 - 1.31$ and $1.48 - 1.90$, for the different polarizations in the NLOS and LOS case, respectively. With such small K-factors, at least the NLOS measurements can be approximated to have a Rayleigh distribution. Here, it is worth mentioning again that the LOS scenario also includes cases where the (patch) antennas are not aimed at each other and cases where the person using the device under test, depending on the actual "working position", obstructs the direct path.

C. Correlation at Tx and Rx

1) Static Measurements: A key characteristic of MIMO channels is the correlation between the entries of the impulse response matrix. A full description of those correlations requires a correlation matrix of size $N_r N_t \times N_r N_t$, which is reasonable for the considered systems; For the FD-PC scenario, we analyze the correlation at receiver and transmitter for 4×4 (i.e., 2 dual-polarized $\times$ 2 dual-polarized) MIMO systems. For the FD-HH and PC-HH measurements we analyze 4×2 MIMO systems. The 4 antennas at the Tx/Rx are labelled v(ertical) 1 and 2, and h(orizontal) 1 and 2. The mean and standard deviation of the magnitude of the (complex) correlation coefficient between different antennas at the Tx is given in Table IV, while values for the correlation between different antennas at the Rx is given in Table V. Due to space restrictions we can, however, not present the full correlation matrix in the paper.

2) Dynamic Measurements: To determine the coherence time of the channel we calculated the correlation coefficients of the entries in the transfer function matrix for the dynamic measurements over an interval where the channel was assumed to fulfil wide-sense stationarity, uncorrelated scattering (WSS-US) conditions. The walking speed of 1.5 m/s (see Section II-C) corresponds to a maximum Doppler frequency of 13 Hz. In Fig. 8 we present correlation coefficients from 5 different measurements. From the measurements it can also be noted that the different polarizations have similar behavior. The coherence times are estimated to $T_{|\rho|=0.9} = 12$ ms and $T_{|\rho|=0.5} = 35$ ms for the PC-HH scenario. When the antennas are static and there is only movements in the corridor, the channel changes are very small.

TABLE IV

MAGNITUDE OF CORRELATION COEFFICIENTS AT THE TRANSMITTER.

		FD-PC		FD-HH		PC-HH	
		$m_{\|\rho\|}$	$\sigma_{\|\rho\|}$	$m_{\|\rho\|}$	$\sigma_{\|\rho\|}$	$m_{\|\rho\|}$	$\sigma_{\|\rho\|}$
LOS:	h1-v1	0.07	0.05	0.14	0.11	0.02	0.01
	v1-h2	0.07	0.06	0.13	0.07	0.03	0.02
	h1-v2	0.07	0.05	0.11	0.08	0.02	0.01
	h1-h2	0.27	0.13	0.34	0.20	0.05	0.04
	v1-v2	0.24	0.10	0.18	0.12	0.06	0.05
NLOS:	h1-v1	0.06	0.04	0.05	0.03	–	–
	v1-h2	0.07	0.04	0.06	0.04	–	–
	h1-v2	0.06	0.04	0.05	0.03	–	–
	h1-h2	0.34	0.15	0.34	0.17	–	–
	v1-v2	0.16	0.09	0.15	0.10	–	–

TABLE V

MAGNITUDE OF CORRELATION COEFFICIENTS AT THE RECEIVER.

		FD-PC	
		$m_{\|\rho\|}$	$\sigma_{\|\rho\|}$
LOS:	h1-v1	0.10	0.07
	v1-h2	0.13	0.09
	h1-v2	0.15	0.11
	h1-h2	0.15	0.10
	v1-v2	0.16	0.10
NLOS:	h1-v1	0.10	0.06
	v1-h2	0.13	0.07
	h1-v2	0.13	0.09
	h1-h2	0.19	0.13
	v1-v2	0.13	0.09

IV. SUMMARY AND CONCLUSIONS

We presented the results of an extensive measurement campaign for MIMO wireless propagation channels. The scenarios, antenna arrangements, and choice of locations correspond to typical PANs, covering situations with fixed devices, PCs, and PDAs. We draw the following conclusions:

- Pathloss can be modeled by the classical "power-distance law" and shadowing by a lognormally distributed random variable. However, in the distance range considered for PANs, the impact of the distance dependence is minor, and shadowing dominates.
- The definition of "LOS" becomes ambiguous, as the obstruction of a direct propagation path between Tx and Rx can be due to the mounting of the antenna, or the person holding the device.
- For the power delay profile, only a single exponential cluster was observed.
- The decay time constant can be modeled as a random variable, but does not show a distance dependence.
- The correlations between the entries of the transfer function matrix are low, with a mean of generally less than 0.2, both between co-located antennas with different polarizations, and between antennas separated by about half a wavelength, but having the same polarization.

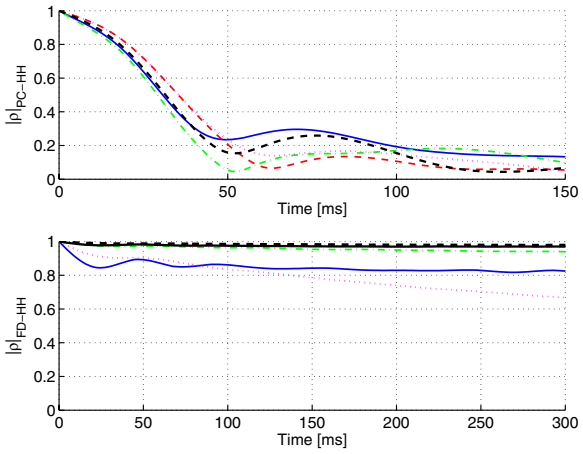

Fig. 8. Correlation coefficient as a function of time for 5 measurements. The top figure is for the PC-HH measurements, were the HH was moving, the lower figure is for the FD-HH measurement were the devices were static and a person was walking along the corridor.

- The coherence time of the channel is reasonably large, especially for the case of static devices in a temporally varying surrounding, but also for the case of moving devices.

These results can be used to provide a realistic model for many PAN scenarios. Another interesting case, that of body-worn devices, could not be presented here for space reasons, and will be elaborated on in a forthcoming paper.

ACKNOWLEDGEMENTS

Part of this work was funded from the MAGNET project (contract no. 507102) of the European Union, an INGVAR grant of the Swedish Foundation for Strategic Research, and a grant from the Swedish Science Council.

REFERENCES

[1] A. Batra et al, "Multi-band OFDM physical layer proposal," 2003. Document IEEE 802.15-03/267r2.

[2] J. McCorkle et al, "Xtreme spectrum cpf document," 2003. Document IEEE 802.15-03/154r0.

[3] G. J. Foschini and M. J. Gans, "On limits of wireless communications in a fading environment when using multiple antennas," *Wireless Personal Communications*, vol. 6, pp. 311–335, Feb. 1998.

[4] I. E. Telatar, "Capacity of multi-antenna Gaussian channels," *European Transactions on Telecommunications*, vol. 10, November-December 1999.

[5] A. Paulraj, D. Gore, and R. Nabar, *Multiple Antenna Systems*. Cambridge, U.K.: Cambridge University Press, 2003.

[6] D. Gesbert, M. Shafi, D.-S. Shiu, P. J. Smith, , and A. Naguib, "From theory to practice: An overview of MIMO space-time coded wireless systems," *IEEE J. Selected Ares Comm.*, vol. 21, pp. 281–302, 2003.

[7] A. F. Molisch and F. Tufvesson, "MIMO channel capacity and measurements," in *Smart Antennas - state of the art* (T. Kaiser, ed.), Eurasip publishing, 2005.

[8] 3GPP-3GPP2 Spatial Channel Model Ad-hoc Group, "Spatial channel model for MIMO systems," tech. rep., 2003. 3GPP and 3GPP2; download at http://www.3gpp.org.

[9] V. Erzeg, L. Schumacher, P. Kyritsi, D. S. Baum, A. F. Molisch, and A. Y. Gorokhov, "Indoor MIMO WLAN channel models," in *Standardization drafts of IEEE 802 meeting*, (Dallas, USA), Mar. 2003.

[10] M. Steinbauer, A. F. Molisch, and E. Bonek, "The double-directional radio channel," *IEEE Antennas and Propagation Magazine*, vol. 43, pp. 51–63, Aug. 2001.

[11] J. Medbo, J.-E. Berg, and F. Harryson, "Temporal radio channel variations with stationary terminal," in *Proc. 60th IEEE Vehicular Technology Conference*, Sept. 2004.

[12] B. H. Fleury, M. Tschudin, R. Heddergott, D. Dahlhaus, and I. K. Pedersen, "Channel parameter estimation in mobile radio environments using the SAGE algorithm," *IEEE J. Selected Areas Comm.*, pp. 434–450, 1999.

[13] M. Haardt and J. A. Nossek, "Unitary ESPRIT: How to obtain increased estimation accuracy with a reduced computational burden," *IEEE Trans. on Signal Proc.*, vol. 43, pp. 1232–1242, May 1995.

[14] R. Thomae, D. Hampicke, A. Richter, G. Sommerkorn, A. Schneider, U. Trautwein, and W. Wirnitzer, "Identification of the time-variant directional mobile radio channels," *IEEE Trans. on Instrumentation and measurement*, vol. 49, pp. 357–364, 2000.

[15] A. Saleh and R. A. Valenzuela, "A statistical model for indoor multipath propagation," *IEEE J. Selected Areas Comm.*, vol. 5, pp. 138–137, Feb. 1987.

[16] L. J. Greenstein, D. G. Michelson, and V. Erceg, "Moment-method estimation of the Ricean K-factor," *IEEE Communications Letters*, vol. 3, pp. 175–176, June 1999.